Analytical Methods

ROYAL SOCIETY OF CHEMISTRY

PAPER

View Article Online
View Journal

Cite this: DOI: 10.1039/d6ay00498a

The development of aptamer-functionalized streptavidin magnetic particles for sample purification of SARS-CoV-2 coupled with rapid plasmonic RT-qPCR to improve detection sensitivity

Joshua Hayes,†[a] Alex Resendes,†[ab] Seung Soo Lee,[ab] Mitra Yousefi,[cd] Silvia Vidal,[cd] Miltiadis Paliouras *[ae] and Mark Trifiro*[abe]

Despite having endured numerous pandemics throughout history and contemporary technological advancements, the world was still unprepared for the emergence of the SARS-CoV-2 pathogen. Prior to the development and distribution of effective vaccines, health officials relied heavily on diagnostics to contain the spread of the virus. Reverse transcription-polymerase chain reaction (RT-PCR) is employed for diagnosing SARS-CoV-2 due to its exceptional sensitivity and specificity. However, clinical sample preparation techniques for SARS-CoV-2 may have limited detection sensitivity due to the large volumes of viral transport medium in which nasopharyngeal swabs are stored, and where only a fraction of the sample was used for analysis. Consequently, we have developed a sample processing method that improves the sensitivity and specificity of SARS-CoV-2 diagnostics by capturing viral particles using aptamers specific to the S-protein functionalized on magnetic particles ("apta-beads") and thereby concentrating the analyte. The eluted viral particles are then directly amplified on the Kimera P-IV point-of-care plasmonic qPCR platform. With our protocols, we have been able to capture various forms of SARS-CoV-2 analytes, including recombinant spike protein from both Wuhan and Omicron strains, spike-expressing pseudoviral particles, and SARS-CoV-2 viruses. Furthermore, the capture protocol can be performed in as little as 2 minutes, with the added effect of removing unwanted inhibitory components to PCR reactions. In conclusion, our "apta-bead" sample purification, combined with the rapid plasmonic PCR analysis, can play a critical role in limiting sample-to-result turnover time, and thereby mitigate the spread of the infectious disease.

Received 19th March 2026
Accepted 13th May 2026

DOI: 10.1039/d6ay00498a

rsc.li/methods

1. Introduction

The emergence of SARS-CoV-2 highlighted the world's unpreparedness in dealing with a novel viral pathogen, notably when it came to diagnostics. As of April 2024, the COVID-19 pandemic has resulted in over 704 million infections and over 7 million deaths (https://www.worldometers.info/coronavirus/).[1] At the height of the pandemic with the emergence of the Omicron strain in January 2022, almost 4 million infections per day were cataloged worldwide. Despite decades of experience with disease outbreaks, including multiple global epidemics and the development of containment protocols, SARS-CoV-2 still spread rapidly. In the context of the COVID-19 pandemic, prior to the development of the vaccines, diagnostics played the most critical role in infection control by identifying infected individuals, both symptomatic and asymptomatic, and providing isolation directives to reduce further disease transmission. Even after the distribution of the vaccines, diagnostics continued to remain a valuable tool for limiting the dissemination of the disease, given the global COVID-19 vaccine acceptance rate was only 60%.[2]

The "gold" standard for assessing a COVID-19 infection is *via* reverse transcriptase PCR (RT-PCR) analysis as it provides superior specificity and sensitivity to diagnose acute infection;[3] however, a major limitation of SARS-CoV-2 diagnostics during the pandemic was the prolonged test-to-result turnover time, ranging from 24 to 72 hours, as they were solely conducted in centralized testing laboratories.[4] At the beginning of the pandemic, it could take up to a week to receive a test result.[5] During peak periods of infection, notably during new variant

[a]*Lady Davis Institute for Medical Research – Jewish General Hospital, Montreal, QC, Canada. E-mail: miltiadis.paliouras@mcgill.ca; mark.trifiro@mcgill.ca*
[b]*Division of Experimental Medicine, McGill University, Montreal, QC, Canada*
[c]*Human Genetics, McGill University, Montreal, QC, Canada*
[d]*McGill University Life Sciences Complex, Montreal, QC, Canada*
[e]*Department of Medicine, McGill University, Montreal, QC, Canada*
† These authors contributed equally to this work.

waves, healthcare systems became overwhelmed by the volume of test requests and by shortages in supplies, therefore limiting RT-PCR testing to vulnerable groups.[6] It is also suggested that the sensitivity of RT-PCR testing could be affected by the changing genome of the Omicron variant sub-lineages.[7] Ultimately, the rest of the population was confined to the use of home testing kits, which lack substantial sensitivity; thus, asymptomatic individuals and people in the early stages of infection could have received a false-negative result, allowing them to unknowingly transmit the virus.

Another major limitation of the testing protocol stems from the sub-optimal clinical specimen processing that occurs before RT-PCR analysis. An example of this is Roche's SARS-CoV-2 Cobas® 8800 system, which was given Emergency Use Authorization by the Food and Drug Administration during the pandemic.[8] Firstly, nasopharyngeal swabs collected from infected patients are submerged in 3 mL of universal viral transport medium or 0.9% physiological saline, yet only 400 μL is used for the nucleic acid isolation step – equivalent to roughly one-eighth of the original patient sample.[9] Next, the lysis buffer that releases the viral genetic material introduces potential RT-PCR inhibitors to the sample including guanidine thiocyanate, polidocanol, and dithiothreitol.[10–12] To capture the viral RNA, glass magnetic beads are added; however, they lack any target specificity.[13] This is problematic because it also co-purifies non-viral nucleic acids from nasal epithelial cells, thereby diluting the total target viral RNA concentration. The washing steps are aimed at removing PCR inhibitory components, followed by a final elution step which results in a combination of virus and epithelial cells. Roughly, 5 μL of the processed sample is added into the PCR mix, and this automated process, from RNA extraction to RT-PCR analysis, can take nearly 4 hours to complete.[14,15]

More than 70% of the infectious agents that infect humans are of viral origin;[16] therefore, it would be useful to have a tool that can purify the virion from complex clinical samples. Consequently, we developed an approach that can capture a specific viral target while preserving the diagnostic sensitivity of the benchmark RT-PCR system. We began by selecting streptavidin magnetic particles (SMPs) onto which we attached aptamer probes developed specifically to the S-protein on SARS-CoV-2, as these beads are frequently used in capture assays and are highly efficient at separating unique molecules from complex mixtures. These S-protein aptamer-functionalized SMPs (apta-beads) selectively capture and concentrate the viral particles instead of contaminant cells. The eluted sample, enriched with only viral RNA, is directly tested on the Kimera P-IV point-of-care plasmonic qPCR platform.[17,18] In sum, we demonstrate that our Apta-bead protocol provides an advancement for diagnostics by simultaneously purifying and concentrating the target pathogen, leading to greater detection sensitivity and specificity.

2. Materials and methods

2.1 Aptamer design

Four SELEX-selected nucleic acid DNA sequences, capable of folding into secondary/tertiary structures and binding targets based on their 3-dimensional conformation rather than just their complementary sequence, were identified as potential aptamer candidates. A list of every aptamer sequence tested can be found in Table 1. Each unique sequence was developed by an independent research group and can bind the SARS-CoV-2 spike protein in some capacity, whether on the receptor-binding domain or somewhere else on the spike S1 subunit.[19–22] Each sequence was modified to include a terminal biotin moiety at either the 3′ end (/3Bio/) or the 5′ end (/5Biosg/), with an internal

Table 1 List of Apta-beads[a]

AB	Size (bp)	Sequence (5′–3′) (1)	Target	K_d (nM)	Ref.
AB1	51	CAG CAC CGA CCT TGT GCT TTG GGA GTG CTG GTC CAA GGG CGT TAA TGG ACA/iSp18//3Bio/	SARS-CoV-2 spike RBD	5.8	21
AB2	45	CCC GAC CAG CCA CCA TCA GCA ACT CTT CCG CGT CCA TCC CTG CTG/iSp18//3Bio/	Active SARS-CoV-2 spike	79	19
AB3	24	GGG GTG GGG TAG TGG TAT GGA GCG/iSp18//3Bio/	SARS-CoV-2 spike S1	4.26	20
AB4	40	CCG CAG GCA GCT GCC ATT AGT CTC TAT CCG TGA CGG TAT G/iSp18//3Bio/	SARS-CoV-2 spike RBD	0.33	22
AB1-5Bio	51	/5Bio//iSp18/C AGC ACC GAC CTT GTG CTT TGG GAG TGC TGG TCC AAG GGC GTT AAT GGA CA	SARS-CoV-2 spike RBD		
AB1-3Bio+15T	66	CAG CAC CGA CCT TGT GCT TTG GGA GTG CTG GTC CAA GGG CGT TAA TGG ACA TTT TTT TTT TTT TTT/iSp18//3Bio/	SARS-CoV-2 spike RBD		
AB1-5Bio+15T	66	/5Bio//iSp18/TTT TTT TTT TTT TTT CAG CAC CGA CCT TGT GCT TTG GGA GTG CTG GTC CAA GGG CGT TAA TGG ACA	SARS-CoV-2 spike RBD		

[a] (1) Oligonucleotide modifications (shown in bold): internal hexa-ethylene glycol spacer (iSp18), 3′ biotin (3Bio) and 5′ biotin (5Bio), 15 thymine bases (15T).

hexa-ethylene glycol spacer region (/iSp18/) directly adjacent to it. Furthermore, some of the sequences were designed with an additional 15 nucleotide-long thymine extension on either 3′ or 5′ ends. The modifications made to the aptamers should have a neutral effect on their pulldown affinity.[23–25] All nucleic acid sequences were modified and produced by Integrated DNA Technologies (Coralville, USA).

2.2 Apta-bead preparation

The conjugation of the previously described biotin-labelled aptamer sequences onto streptavidin magnetic particles (Roche *via* MilliporeSigma, Burlington, USA) was performed according to the manufacturer's protocol. As per the manufacturer's specifications, the particles have a mean diameter of 1 μm, a specific gravity within the range of 1.1–1.4 g cm^{-3} and a free biotin binding capacity of ∼1800 pmol mg^{-1}. A 200 μL aliquot of the streptavidin magnetic particle suspension stock (10 mg mL^{-1}) was added to a 1.5 mL microcentrifuge tube. These magnetic particles were washed three times using TEN100 buffer (10 mM Tris, 100 mM NaCl, 1 mM EDTA, pH = 7.5). Tris, NaCl, and EDTA solutions were made by diluting respective molecular grade powders in d_2H_2O and subsequently adjusting the pH according to manufacturer specifications, then autoclaved. Washes consisted of adding 400 μL of buffer to the microcentrifuge tube, vortexing for 5 seconds, placing the tube on a magnetic separation rack for 40 seconds, and removing the supernatant. During this process, the magnetic particles remained immobilized on the wall of the microcentrifuge tube closest to the magnet of the Cytiva MagRack™ 6 (Marlborough, USA). Following these three washes, another 400 μL of TEN100 was added to the microcentrifuge tube containing only the washed magnetic particles aggregated on the side of the tube. The tube was then removed from the magnetic rack and vortexed for 3 seconds to resuspend the magnetic particles in solution.

Additionally, a 50 μL aliquot of the selected aptamer stock (100 μM) was heated to 95 °C for 5 minutes and cooled at room temperature for 10 minutes, to ensure that the aptamer folded into its proper conformation. 30 μL of this primed aptamer was then added to the beads resuspended in TEN100. The aptamer concentration was calculated to be in excess relative to the magnetic particles' biotinylated oligonucleotide binding capacity of 150 pmol mg^{-1} to ensure the complete saturation of every available streptavidin binding spot. This solution containing the aptamers and magnetic particles in suspension was incubated at room temperature for 30 minutes on a tube rotator. This solution, now containing the aptamer-functionalized magnetic particles, underwent another three washes using 400 μL of TEN1000 (10 mM Tris, 1000 mM NaCl, 1 mM EDTA, pH = 7.5). This was followed by two 400 μL washes using immunoprecipitation (IP) buffer (50 mM Tris, 50 mM NaCl, 1 tablet cOmplete™ Mini Protease Inhibitor cocktail (MilliporeSigma, Burlington, USA), pH = 8.0), and a final resuspension in 200 μL. This stock solution (10 mg mL^{-1}) of Apta-beads (AB) was finally diluted to a working solution of 1 mg mL^{-1}. Several batches of ABs were prepared to reproduce results for experiments carried out in the subsequent investigations.

2.3 Inhibition of SMPs and ABs on Kimera P-IV point-of-care plasmonic qPCR

SMPs and/or ABs with masses of 25, 13.2, 6.6, 3.3, and 1.6 μg were added to 20 μL plasmonic PCR reaction mixtures, either DNA-positive reactions containing ∼10^3 copies/reaction *C. trachomatis* DNA (American Type Culture Collection, Manassas, VA, USA), or DNA-negative no-template controls. No-SMP and -AB controls both positive and negative for *C. trachomatis* DNA were also included. 45 cycles of PCR were conducted on 2 repeats of the 25 μg condition and 4 repeats of the other conditions in both the Kimera P-IV point-of-care plasmonic qPCR platform and a conventional thermocycler. Additional conventional PCRs were done with 10^3 *C. trachomatis* DNA samples containing 25 μg of SMPs [CHAI open qPCR platform (CHAI, Santa Clara, USA)]. Melting curve analysis was done after amplification to confirm amplicon generation. Gel electrophoresis was used to validate inhibition of the 25 μg condition, and multi-curve output signal plotting was used to demonstrate dose-dependent inhibition for the other conditions.

2.4 AB capture of SARS-CoV-2

Three different targets were captured with ABs: recombinant SARS-CoV-2 His-tagged spike proteins, purchased from R&D Systems (Minneapolis, USA), SARS-CoV-2 pseudoviruses (eENZYME, Gaithersburg, MA, USA), or SARS-CoV-2 viruses. Various experiments were conducted both under "ideal" and "clinical" conditions. Ideal conditions involved capturing targets in IP buffer only, and clinical conditions involved cell culture media, EDTA, urine, or swab-diluted IP buffer. Urine and swab samples were voluntarily collected from three individuals.

Unless indicated otherwise, the general capture process involved adding target-dependent quantities of ABs to 1.5 mL of various target-containing solutions and left to incubate for 30 minutes at room temperature. 15 minutes into the incubation period, the solution was vortexed for 3 seconds. After incubation, the solution was placed on a magnetic separation rack and left there for 40 seconds, allowing all the virus-bound ABs to pellet to the side of the tube closest to the magnet. The supernatant, containing unbound target and undesirable components such as non-viral genetic material, cellular debris, and PCR inhibitors, was then removed by pipetting. Since the SMPs are polydisperse core–shell polystyrene particles that can potentially induce non-specific interaction with other biomacromolecules, four washing steps were carried out: two using harsh wash buffer (50 mM Tris, 1 M NaCl, 5 mM EDTA, 1 protease inhibitor cocktail tablet, 0.1% v/v Triton (X-100), pH = 7.5) and two using the IP buffer. Each wash involved adding 500 μL of buffer to the virus-AB immobilized pellet, vortexing the solution for 5 seconds, and subsequently leaving it to sit for 40 seconds on the magnetic separation rack. Once all washes were done, the ABs were resuspended in 50 μL of IP buffer and heated for western blot or RT-PCR analysis.

2.4.1 Recombinant SARS-CoV-2 His-tagged spike protein. A 5 : 1 AB to protein ratio was used for capture. Following a pulldown of 100 and 50 ng of recombinant SARS-CoV-2 His-tagged spike protein according to the protocol in Section 2.4, the

final resuspended 50 μL sample was treated with 10 μL of Laemmli buffer containing β-mercaptoethanol (6×) and heated at 95 °C for 5 minutes. After conducting 8% sodium dodecyl-sulfate polyacrylamide gel electrophoresis (SDS-PAGE), the gel was transferred to a nitrocellulose membrane and blocked using 2% skimmed milk in Tris-Buffered Saline (TBS) for an hour at room temperature. All subsequent incubation and washing steps were carried out on a rocking shaker. First, the blot was incubated with a mouse-derived His-tag primary antibody (R&D Systems) overnight at 4 °C at a final antibody concentration of 0.2 μg mL^{-1}, then washed three times (10 minutes each wash) using TBS with Tween-20 (TBST). A horseradish peroxidase-conjugated anti-mouse IgG (Cytiva *via* Cedarlane, Burlington, ON, Canada) secondary antibody, final concentration diluted 2000-fold, was then incubated with the blot for 1 hour at room temperature before undergoing another three 10-minute washes. Blot analysis began with the incubation of the blot with 3 mL of Solution A (luminol) and 3 mL of Solution B (peroxide) from the Amersham ECL Prime Western blotting detection reagent kit (Cytiva) for 5 minutes at room temperature. Lastly, the blot was imaged using a ChemiDoc paired with Image Lab software. The molecular mass (kDa) of each signal was determined based on the Amersham ECL Rainbow MarkerTM (Cytiva). Experiments describing recombinant protein pull-downs were performed 4 times.

2.4.2 SARS-CoV-2 S-protein expressing pseudovirus. The SARS-CoV-2 pseudoviral particles used in this study emulate the S-protein of the Wuhan-Hu-1 strain. They are replication-deficient murine leukemia viruses that express the SARS-CoV-2 S protein, and the top-stock titre was quantified by the manufacturer as $\sim 1 \times 10^8$ pseudoviral particles per mL. From this stock, we correspondingly added 75 000, 7500, 750, or 75 virions into 1.5 mL volumes of solution. The genetic material encapsulated within each virion contains the firefly luciferase RNA sequence. Following the pulldown of this pseudovirus according to the protocol in Section 2.4, the final resuspended 50 μL sample underwent a 95 °C denaturation step for 5 minutes to destabilize the virions, in turn releasing their genetic material. The no-pulldown control used consisted of equivalent pseudoviral particles suspended in 1.5 mL solution, of which 5 μL of both the heat-treated pulldown resuspension in IP buffer and the no-pulldown control were added into 20 μL reaction mixtures for subsequent RT-PCR analysis in the point-of-care plasmonic qPCR platform. All pseudovirus experiments were performed 3-times.

2.4.3 SARS-CoV-2 virus. SARS-CoV-2 clinical isolate virus was propagated, handled, captured, heat inactivated, and quantified according to established protocols.[26] This work was carried out at Biosafety Containment Level 3 facility, McGill Bellini Life Science Complex. The clinical isolate top-stock titre was quantified at $\sim 1.77 \times 10^7$ PFU mL^{-1} and bears strong similarity to the Wuhan-Hu-1 sequence, NC_045512, containing the D614G mutation present in all variants of concern and notably linked to an increase in virus transmissibility.[27] Working stock dilutions were made by taking 90.40 μL of the top-stock and diluting it in 1109.60 μL IP buffer. 75 μL of this stock was taken to achieve 1×10^5 PFU, whereas 75 μL of a 1000× dilution of the working stock in IP buffer was taken to achieve 1×10^2 PFU. A heat inactivation protocol was validated to ensure that the virus was fully inactivated after undergoing a 5-minute denaturation at 95 °C. 1 mL of IP buffer spiked with 10^2 or 10^5 plaque-forming units (PFU) of the virus was used for pulldown. The final 50 μL resuspended mixture containing captured virus underwent this inactivation protocol, thereby releasing the encapsulated viral RNA, and 5 μL of this resuspension subsequently underwent RT-PCR amplification in the point-of-care plasmonic qPCR platform. Each SARS-CoV-2 clinical isolate pulldown was performed 3 times.

2.5 Kimera P-IV 4-channel point-of-care plasmonic RT-PCR protocol

The plasmonic qPCR reaction mixture reagents used for RT-PCR are as follows: PEGylated gold nanorods (GNR) (Nanopartz, Loveland, CO, USA), Taq DNA Polymerase (New England Biolabs, Whitby, ON, Canada), ProtoScript II Reverse Transcriptase and Reaction Buffer (New England Biolabs, Whitby, ON, Canada), dNTPs (Thermo Fisher Scientific, Saint-Laurent, QC, Canada), SYTO-16 (Thermo Fisher Scientific, Saint-Laurent, QC, Canada), Murine RNase Inhibitor (New England Biolabs, Whitby, ON, Canada), and different primer sets (Integrated DNA Technologies, Coralville, IA, USA). Primers used in the RT-PCR protocol are listed in Table 2. Reverse transcription was conducted at 45 °C and held for 10 minutes, followed by an initial denaturation at 85 °C for 1 minute, and lastly 40 cycles of 85 °C denaturation for 10 seconds, 55 °C annealing for 10 seconds, and 68 °C elongation for 10 seconds. To verify the amplification products, 12 μL of post-PCR samples were run on a 2% agarose gel. Amplicon base pair lengths were known and compared to GeneRuler Express DNA Ladder (ThermoFisher). The gel containing a fluorescent DNA/RNA staining solution, purchased from ZmTech (Montreal, Canada), was imaged with a ChemiDoc and visualized using Image Lab software. Unless specified otherwise, all PCR reactions were conducted in this platform.

2.6 Data analysis

Raw data analysis was conducted using a custom python script, including curve fitting, multi-curve plotting, and C_t value detection. C_t values were determined by protocols introduced in our previous publication.[17] Statistical assessments on SMP inhibition on the Kimera P-IV platform output fluorescent signal and C_t values were conducted using a non-parametric Kruskal–Wallis test and a post–hoc Dunn test using a Bonferroni correction.

2.7 Live subject experiments

All experiments were performed in compliance with institutional guidelines of McGill University and the Lady Davis Institute for Medical Research. All subjects voluntarily consented to provide urine or nasal samples.

Table 2 Primer sequences used in plasmonic PCR[a]

Primer (1)	Sequence	Amplicon size (bp)	Melting temperature (°C)
MLV-F	CGGAAAGACGATGACGGAAA	130	55.1
MLV-R	CGGTACTTCGTCCACAAACA		55.0
N7-F	GGGAGCAGAGGCGGCAGTCAA	150	64.4
N7-R	TCAAGCAGCAGCAAAGCAAGAGCA		61.9
CTC6-F	AGTCCTCTAGTACAAACACCCCCA	300	59.1
CTC6-R	TCGCCCGCACGTTCTCTCAA		61.7

[a] (1) MLV primers, pseudovirus luciferase construct; N7 primers, SARS-CoV-2 *N*-gene; CTC6, *C. trachomatis* cryptic plasmid[17]

3. Results and discussion

3.1 Apta-bead design

Aptamers directed at the SARS-Cov-2 S-protein of the Wuhan strain were selected from the literature and were modified accordingly at the 3′-end with PEG spacers and a biotin moiety (see Table 1). As part of the selection process, we chose aptamers with low dissociation constants (K_D) indicating higher binding affinity for the S-protein, as shown by other investigators.[28] The PEG spacer, consisting of 18 internal hexa-ethylene glycol residues, aimed to reduce aptamer SMP steric hindrance. Each SMP is coated with streptavidin, which preferentially and stably binds the biotin moiety of the aptamer, creating the Apta-bead (Fig. 1A). With an average diameter of 1 μm, one SMP is roughly 1000 times the volume of a SARS-CoV-2 virion, allowing multiple viruses to bind each SMP; therefore, the quantity of ABs used will always be sufficient to capture all virus equivalents.[28] Following this assumption, there would always be an excess of aptamer compared to the target S-protein. Numerous reports claim that the number of S-protein per SARS-CoV-2 virion varies from 25 to 100, although the average is closer to the lower extremity of 48 per virus.[29,30] Furthermore, an average SARS-CoV-2 infected sample contains more than 10^6 copies of viral RNA per milliliter.[31] According to

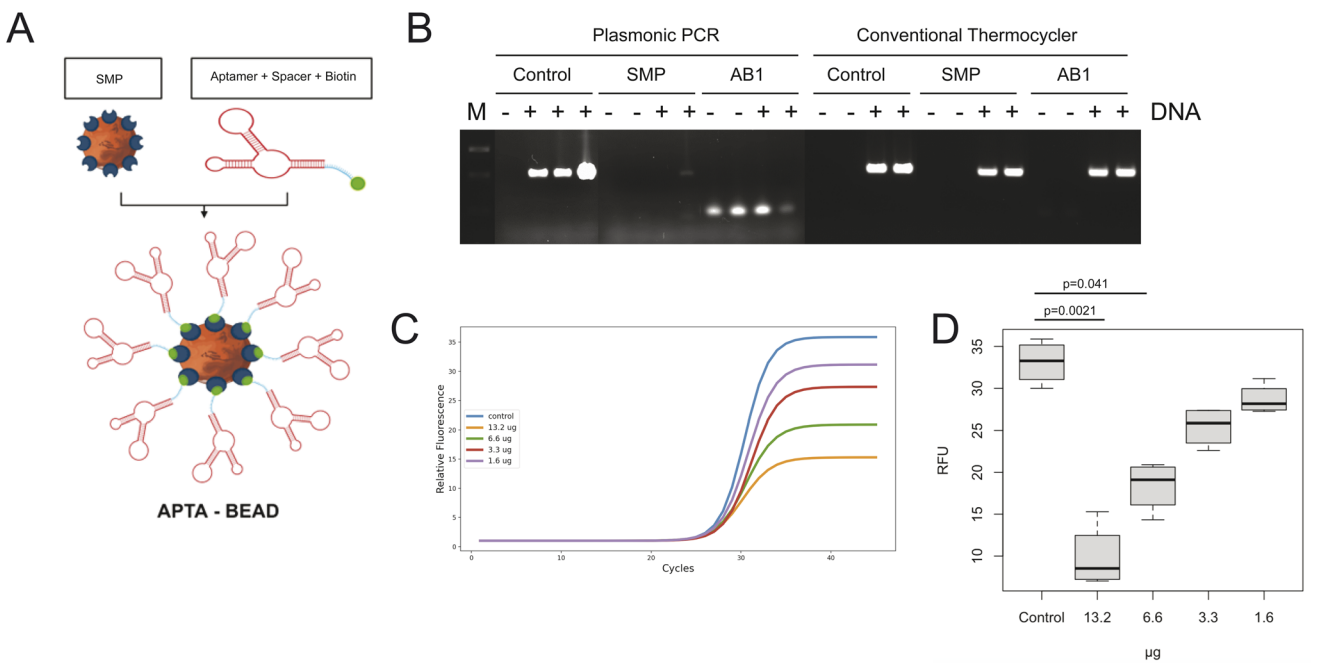

Fig. 1 Characterization of the inhibition of ABs and SMPs on the PCR amplification. (A) Schematic illustrations of an Apta-bead (AB). The image includes the aptamer labelled with biotin and the15-thymine spacer and linked to the SMP forming the functionalized AB. The schematic illustration was created with https://www.biorender.com/. (Agreement number: SF28CGT1L2.) (B) Agarose gel electrophoresis of PCR of *C. trachomatis* samples containing 25 μg of either SMPs or ABs. Strong signal bands at the 300 bp mark represent successful PCR amplification of the intended target. Faint signal bands below the ~100 bp mark represent non-specific PCR amplification, potentially caused by primer dimerization. The presence of SMPs or AB1 in the RT-PCR reaction inhibited plasmonic PCR amplification but did not affect conventional thermal cyclers. Control PCRs indicate that neither AB1 nor SMP was added to the RT-PCR reaction. (C) Kimera P-IV plasmonic qPCR fluorescence output curves of 10^3 copies of *C. trachomatis* amplification containing 13.2 μg, 6.6 μg, 3.3 μg, 1.6 μg and 0 μg of SMPs. (D) Boxplots of relative fluorescence units (RFUs) generated in the Kimera P-IV plasmonic qPCR for 13.2 μg, 6.6 μg, 3.3 μg, 1.6 μg and 0 μg of SMP conditions.

the biotin binding capacity of the SMPs, 25 μg of ABs contain 2.25×10^{12} aptamers, corresponding to roughly 47 000 available aptamers for every S-protein – this can be scaled accordingly.

3.2 Inhibition of ABs and SMPs on Kimera P-IV point-of-care plasmonic qPCR

We observed a clear inhibition of the ABs on the Kimera P-IV amplification that was not observed in a conventional thermal cycler. As seen in Fig. 1B, the gel electrophoresis demonstrates that 25 μg of both bare SMPs and AB1 inhibit PCR amplicon generation on the plasmonic platform, but not the conventional platform. The conventional qPCR control demonstrated that four repeats of the same sample mixture conditions properly amplified in the presence of 25 μg SMPs (SI Data 1). Considering that amplicon generation with the plasmonic PCR was only inhibited with the high concentration of 25 μg of SMPs, we can hypothesize several mechanisms to account for this observation. First, the high concentration of SMPs may perturb the heating properties of the plasmonic PCR by altering the reaction environment. In this scenario, the plasmonic-induced buoyancy-driven convective flow within the reaction volume causes increased motion of all reagents, including SMPs.[32,33] Due to the presence of plasmonic nanoparticles, particle motion within the reaction occurs at a significantly greater extent than in conventional thermocycling platforms, where efficient external heat transfer promotes spatially uniform temperature equilibration and suppresses bulk fluid motion. Consequently, there is a higher probability of SMP–reagent interactions and subsequent inhibitory effects in the plasmonic PCR reaction, further validated by the fact that this was not observed in the plasmonic platform at lower concentrations of SMPs. Secondly, gold nanorods are also highly sensitive to the local dielectric environment; therefore, excessive SMPs could attenuate or redistribute incident light through scattering or absorption, and reduce effective gold nanorod photothermal conversion.[34–36] Another possible contributor is the large concentrations of metal oxide nanoparticles creating reactive oxygen species (ROS) through Fenton-like reactions, compounding the ROS that could already be generated through surface plasmon resonance (SPR) of the GNRs upon incident laser light exposure.[37,38] It is well documented that ROS can oxidize DNA nucleotides leading to substitution mutations,[39–42] and it has been subsequently shown that such lesions significantly hinder PCR amplification efficiency.[43] Additionally, various studies have found that nanoparticle–PCR reagent surface interactions demonstrate inhibitory effects on the reaction.[44–46] Lastly, it is also plausible that high concentrations of these particles, considering their large diameter, interfere with the reaction by overcrowding and interfering with desirable interactions required for amplification.[47,48]

In very small quantities, however, SMPs can be incorporated into plasmonic qPCR reaction mixtures, although they have been shown to impact the PCR efficiency and fluorescence output in a dose-dependent manner. Fig. 1C demonstrates the output fluorescence curves from the Kimera P-IV for various masses (μg) of SMPs added into plasmonic qPCR reaction mixtures containing $\sim 10^3$ copies of *C. trachomatis* DNA. The mean C_t values under the no-SMP control, 13.2 μg, 6.6 μg, 3.3 μg, and 1.6 μg conditions, were 27.57 ± 0.29, 27.46 ± 1.15, 28.72 ± 1.70, 28.32 ± 0.79, and 28.66 ± 1.33, respectively. The Kruskal–Wallis test on the C_t values of the five conditions denoted $p = 0.4258$, indicating no statistically significant differences among groups. Moreover, the mean relative fluorescence unit (RFU) values for the no-SMP control, 13.2 μg, 6.6 μg, 3.3 μg, and 1.6 μg conditions, were 33.11 ± 2.6, 9.84 ± 3.81, 18.37 ± 2.99, 25.42 ± 2.34, and 28.68 ± 1.77, respectively. The Kruskal–Wallis test on the RFU values of the five conditions denoted $p = 0.0016$, indicating statistically significant differences among groups. A post–hoc Dunn test yielded statistically significant differences between the no-SMP control, and the 13.2 μg ($p = 0.0021$) and 6.6 μg ($p = 0.041$) conditions, indicating a dose-dependent relationship between higher magnetic particle concentrations and fluorescence output readings on the plasmonic qPCR platform (Fig. 2D).

The impact on the C_t and RFU results likely indicate that the SMPs mainly affect the fluorescence readings in the plasmonic qPCR platform at low concentrations and therefore do not significantly interfere with DNA amplification. Absorption by the SMPs at both SYTO-16's 488 nm excitation and 525 nm emission wavelengths was confirmed by spectrophotometry (SI Data 2). Consequently, based on the binding capacity of ABs and the interference of SMPs with the plasmonic qPCR assay, we opted to perform subsequent experiments using 25 μg of ABs and to elute bound virions into solution, thereby avoiding the incorporation of SMPs into the PCR reaction mixture.

3.3 Recombinant SARS-CoV-2 His-tagged spike protein isolation

The S-protein is an ideal target because all viable viruses express it, and its abundance across the envelope provides the ABs with multiple opportunities to capture it. Its protrusion from the surface also makes it the most accessible protein, considering that adjacent spikes are estimated to be separated by nearly 15 nm of space.[49] Of the four ABs we created, AB1 and AB4 target the S-protein receptor binding domain (RBD), while AB2 targets the whole S-protein and AB3 targets the S1 subunit.[19–22] Whether using a purified recombinant protein or viral material, the AB pulldowns were carried out as illustrated in Fig. 2 and detailed in the Materials and Methods section. To circumvent the inhibition of the ABs on our plasmonic PCR reaction, we placed the heat-inactivated sample back on the magnet rack, separating the ABs from the eluate containing free-floating viral RNA, before aliquoting a portion of the sample into the RT-PCR reaction mixture.

Our initial AB assisted pulldown studies began with using 100 ng of recombinant SARS-CoV-2 His-tagged S-protein based on the SARS-CoV-2 virion mass estimated by Sender *et al.*[50] A 5 : 1 AB : S-protein ratio was used for our pulldowns of Wuhan strain S-protein, and all aptamers targeted this strain. AB1 was able to capture and retain the S-protein more effectively than any other aptamer as seen in the western blot images in Fig. 3A. Each AB was able to capture the majority of S-proteins present

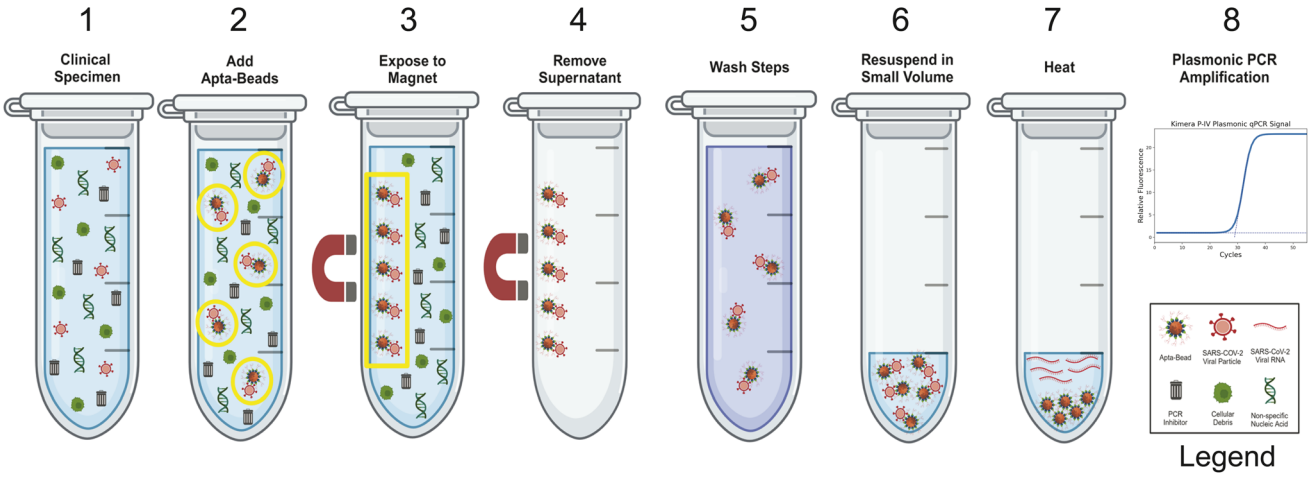

Fig. 2 Schematic illustration of the AB/S-protein pulldown protocol. The steps of protocol include: (1) clinical specimen containing a variety of biological materials, including detection inhibitors. (2) SARS-CoV-2 S-protein specific AB are added to the patient specimen and specifically bind virions. (3) ABs with bound virions are isolated from solution using a magnet. (4) The supernatant is removed, leaving behind ABs and bound virions. (5) Four wash steps are done to remove potential PCR inhibitors. (6) ABs and bound virions are resuspended in a small volume to concentrate the target viral RNA. (7) The sample is heated to release encapsulated viral RNA into solution. (8) Plasmonic RT-PCR analysis conducted on the purified sample resulting in rapid and sensitive diagnoses. Included is a legend of the illustrated components of the AB/S-protein pulldown. The schematic illustration was created with https://www.biorender.com/. (Agreement number: VG28CGTAZM.)

in solution, as supported by the empty supernatant lanes; however, the weaker signals of AB2, AB3, and AB4 compared to AB1, and the positive control indicate that there was a more significant loss of S-protein during the washes. When the highly mutated Omicron variant S-protein was assessed (Fig. 3B), not all the S-protein was captured after the incubation period, as evidenced by the signal observed in the supernatant lanes; however, this is expected as the Omicron variant S-protein is highly mutated compared to the Wuhan strain to which the aptamers were designed against. Nonetheless, AB1 again clearly showed better binding to the Omicron variant S-protein

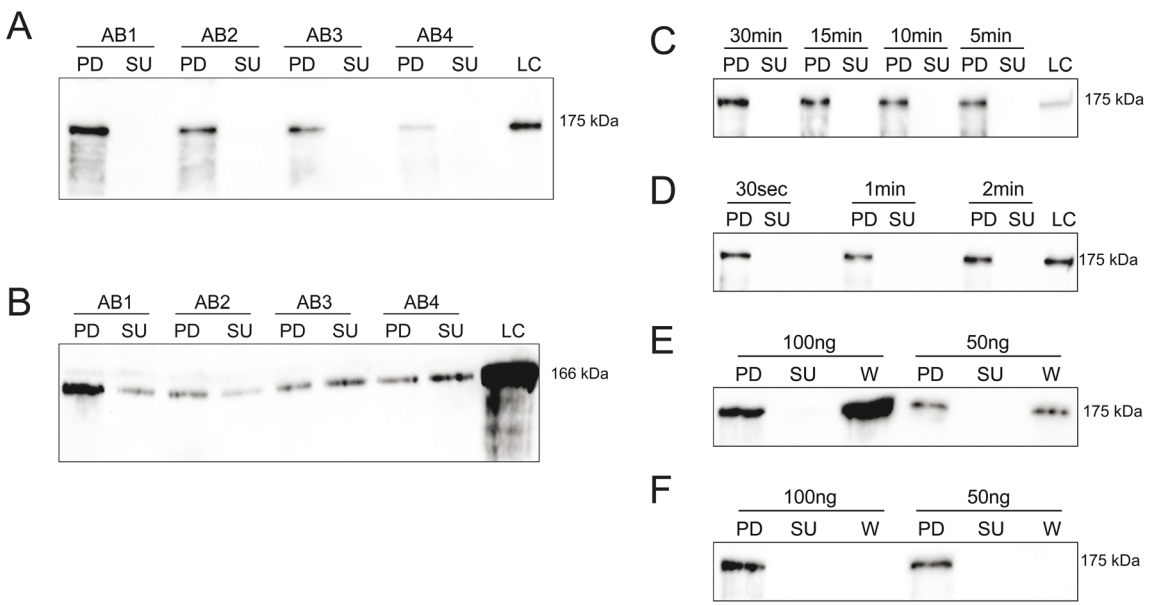

Fig. 3 AB pulldowns of recombinant S-protein. (A) Pulldowns with 100 ng of Wuhan SARS-CoV-2 His-tagged S-protein or (B) 100 ng of Omicron variant SARS-CoV-2 His-tagged S-protein with ABs. The signal bands are located at the appropriate molecular masses of 175 kDa (Wuhan) and 166 kDa (Omicron). All subsequent pulldowns were performed using the 175 kDa Wuhan SARS-CoV-2 His-tagged S-protein using AB1 Apta-beads. (C) Analysis of Apta-bead incubation times (30 min, 15 min, 10 min, or 5 min) given to bind the SARS-CoV-2 spike protein before removing the supernatant. (D) Analysis of magnet exposure time to separate the Apta-beads from the rest of the solution. (E) Analysis of the effect of subsequent washes using a stringent wash buffer. (F) Analysis of the effect of subsequent washes using IP Buffer. Abbreviations: PD, pulldown; SU, supernatant; LC, loading control (purified recombinant S-protein); W, wash.

compared to the others. Accordingly, we have selected AB1 and used them in subsequent experiments.

To optimize the pulldown protocol, we then assessed various incubation times, ranging from 30 minutes down to 5 minutes (Fig. 3C). Results indicate that a 5-minute incubation was sufficient to capture all the S-protein in solution without losing a significant amount of binding after three washes. We subsequently determined that 30 seconds was the time needed for the ABs to migrate to the magnet rack without affecting the S-protein yield (Fig. 3D). We also found that 30 seconds was sufficient for all other AB constructs to move to the wall of the tube before removing the supernatant (data not shown), thus the particles are not perturbed by the selective aptamers on the SMPs, thus differences are solely attributed to the ability of the aptamer to capture the S-protein.

Clinical specimens benefit from washes containing Triton X-100 and EDTA to reduce non-specific binding; thus, pulldowns were performed to compare the intensity of protein capture between the wash buffer containing EDTA and Triton X-100 (Fig. 3E), and IP buffer (without EDTA or Triton X-100) (Fig. 3F) conditions. Given the presence of signal in the wash lanes after using wash buffer, it is obvious that the stringency of these washes removed some S-protein from the ABs; however, a considerable amount of S-protein still remained bound after the three washes with the more stringent buffer. This experiment also validated our ability to perform our pulldown methodology to capture as little as 50 ng of S-protein.

To assess "clinical-like" conditions of the pulldowns, we first introduced ABs into a 50 μL volume containing 10 μL saliva (Fig. 4A). Although AB1 successfully captured the S-protein, there was significant loss after washing three washes with wash buffer. Therefore, to increase the affinity of the AB1, a string of thymine nucleotides were added at either the 5′ or 3′ end along with the location of the Biotin motif.[51] Consequently, in another experiment performed in DMEM cell culture media, containing 10% FBS and 1% penicillin–streptomycin, the following configuration of AB1 with the biotin motif placed on the 5′-end was used (Fig. 4B). The numerous non-specific proteins, especially albumin, bound the western blot antibodies, producing signals at molecular weights other than the expected 175 kDa. The signal in the supernatant lanes suggests that these proteins also interfered with the total binding of all the S-protein starting material. Clean wash lanes further prove that the IP buffer did not disrupt the AB-spike complex. We hypothesize that the proteins interfered with the proper binding between the S-protein and the aptamer by blocking the spike protein's RBD. A considerable amount of the S-protein starting material was still captured, even after three washes with IP buffer. Lastly, a pulldown in 1 mL of 0.9% saline was very successful as no S-protein was observed in the supernatant, using the two configurations: AB1-3′Bio+15T and AB1-5′Bio+15T (Fig. 4C). The bare bead control lane of functionalized SMPs instead of ABs illustrates that there is no significant non-specific binding of the S-protein to the SMPs, reaffirming that the S-protein capture is truly aptamer dependent. Both configurations worked equally well, suggesting the versatility of the aptamer design; however, for the purposes of our subsequent experiments, we selected the AB1-5′Bio+15T configuration.

3.4 SARS-CoV-2 S-protein expressing pseudovirus isolation

Following our recombinant S-protein capture validation experiments, we used murine leukemia pseudovirus expressing Wuhan S-protein on their external surfaces and containing a luciferase RNA construct that we used for RT-PCR validation of our AB pulldowns. Pulldowns with AB1-5′Bio+15T, AB2, AB3, and AB4 configurations were done in a total volume of 1.5 mL with a starting quantity of 500 virions, incubated for 30 minutes, and endured two washes using wash buffer followed by another two washes with IP buffer. The isolated virions were then subsequently amplified *via* RT-PCR on the Kimera P-IV plasmonic qPCR platform. Fig. 5A demonstrates that AB1-5′Bio+15T and AB2 worked well in pulling down whole pseudovirus as observed by the positive RT-PCR product,

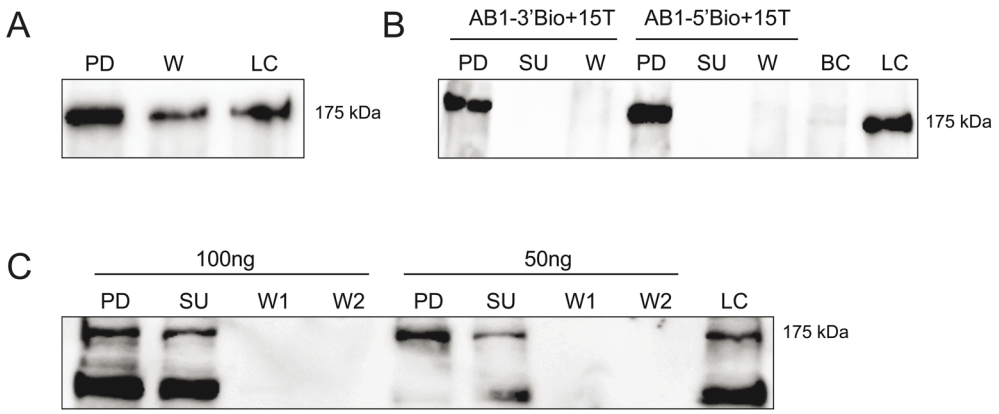

Fig. 4 S-protein pulldowns with optimized ABs in complex solutions. (A) Pulldown of 100 ng S-protein in saliva with AB1. (B) Pulldown of 100 ng of S-protein in 1 mL of 0.9% saline using ABs containing a thymine extension (15T) and biotinylated at the 3′ or 5′ ends. BC is the bead control containing an equivalent amount of non-functionalized SMPs. (C) Pulldown of 100 ng or 50 ng S-protein in cell culture media with AB1-5′Bio+15T and includes two wash steps. The DMEM cell culture media also contains 10% FBS and 1% penicillin–streptomycin. Abbreviations: PD, pulldown; SU, supernatant; LC, loading control (purified recombinant S-protein); W, wash.

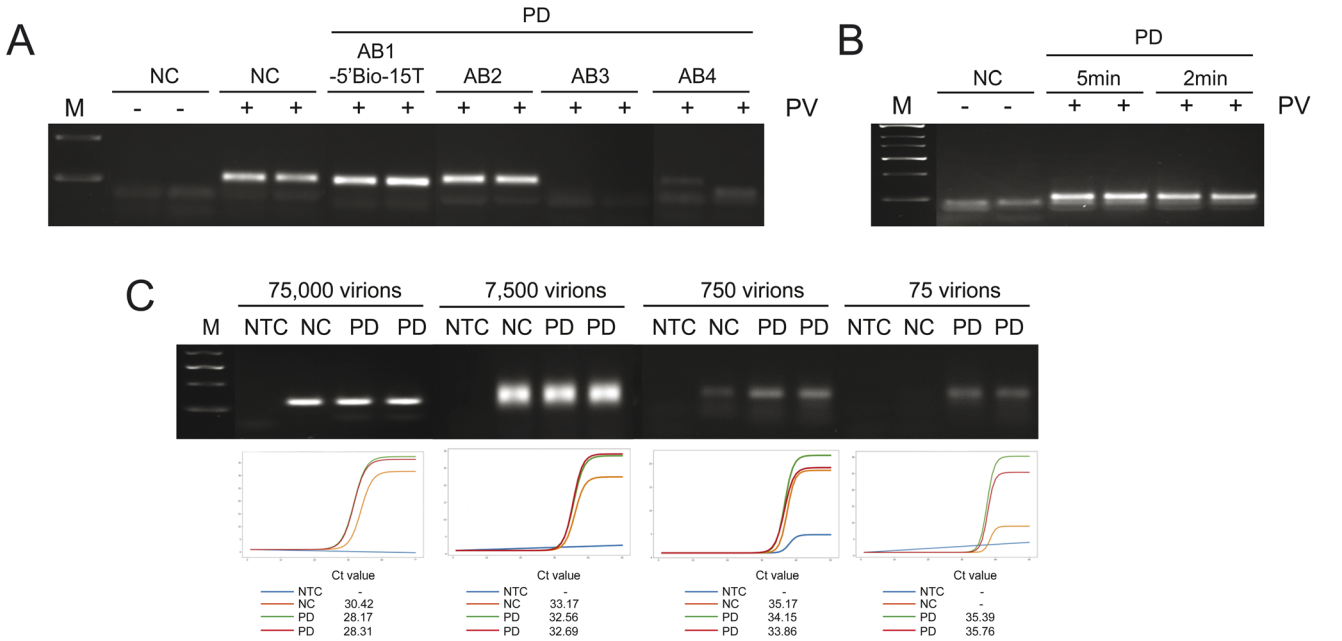

Fig. 5 AB pulldowns of S-protein expressing pseudovirus. (A) S-protein expressing pseudovirus pulldown and subsequent RT-PCR analysis from 4 ABs and results of agarose gel electrophoresis. Negative control is no pseudovirus and positive control is direct RT-PCR analysis of pseudovirus. Amplicon size 130 bp. (B) Varied AB incubation times (5 min or 2 min) using AB1-5′Bio+15T. (C) Plasmonic RT-qPCR output fluorescence curve results, with C_t values of 75 000, 7,500, 750, or 75 pseudovirus pulldowns from 1.5 mL volume, using AB1-5′Bio+15T. Abbreviations: PV, pseudovirus; NTC, no template control; NC, no pulldown control; PD, pulldown.

similar and comparable to the amplicon produced by the pseudovirus positive control. The AB3 and AB4 configurations failed altogether. We also assessed AB1-5′Bio+15T incubation time with pseudovirus, with both 5- and 2-minute conditions yielding successful RT-PCR amplification, indicating that only 2 minutes of incubation time is necessary (Fig. 5B).

Investigators measured the viral loads from saliva samples of university students infected with SARS-CoV-2 and found the mean and median viral loads of the asymptomatic students to be 9.9×10^8 virions per mL and 1.1×10^6 virions per mL, respectively.[52] To emphasize how sensitive our AB pulldown protocol is with the AB1-5′Bio+15T configuration, we performed pseudovirus pulldowns in 1.5 mL of IP buffer containing different concentrations of pseudovirus. Fig. 5C illustrates RT-PCRs of a 75 000 virion pulldown from 1.5 mL volume of IP buffer. The C_t values yielded from the AB pulldown were approximately 28, whereas the no-pulldown control, which represents a 1/300 total virion dilution, yielded a C_t value of 30.42. We also assessed even fewer virions, 7500 (C_t, 32.6), 750 (C_t, 34) and 75 (C_t, 35.6), with our AB pulldown protocol and successfully isolated and concentrated from a 1.5 mL volume. It should be noted that the no-pull down controls (NC) represent a 5 μL isolate from a 1.5 mL volume, or 1/300 fraction of the original sample that is amplified per reaction. Thus, under 75 000 (250 virions/reaction), 7500 (25 virions/reaction) and 750 (~3 virions/reaction) copies/1.5 mL NC conditions, we observed a discernable amplification; however, for the 75 virion condition (0.3 virions/reaction), we did not. Notably, the AB pulldowns effectively isolated and concentrated virions from the 75 virions/1.5 mL sample volume condition, achieving a C_t value of ~35.6. These experiments highlight both the robustness of our protocol when dealing with low viral loads, as well as the innate sensitivity of the point-of-care plasmonic qPCR device. How robust our protocol is when dealing with low viral loads.

We then assessed whether the ABs can capture pseudovirus in complex mixtures known to contain constituents that would inhibit the RT-PCR buffer.[53] Successful pseudovirus pulldowns with AB1-5′Bio+15T, and subsequent RT-PCRs with the Kimera P-IV plasmonic qPCR platform, were performed in 25 mM EDTA-contaminated buffer, urine, and nasopharyngeal swab-dilute buffer. A pulldown of 500 virions in IP buffer containing 25 mM of EDTA gave a C_t value of about 33.5, compared to the no-pulldown control which was completely inhibited (Fig. 6A). This demonstrates that our protocol can remove RT-PCR inhibitors even if concentrated 25-fold more than the standard inhibitory concentration.

Mori *et al.* described how PCR inhibitors present in urine can cause false-negative results in the diagnosis of Toscana virus, another enveloped RNA virus;[54] and although quite uncommon, SARS-CoV-2 has been detected in urine.[55] Consequently, we sought to verify whether known urine-derived PCR inhibitors like urea, high salt concentrations, and elevated protein levels could be eliminated through pulldown sample purification. A pulldown of virion-spiked urine samples achieved a C_t value of roughly 36, whereas the no-pulldown control again had no signal (Fig. 6B), confirming that the pulldown protocol can also overcome the compounded inhibitory effects of urine that would otherwise prevent a proper diagnosis. Finally, the ABs were shown to be effective by successfully capturing virions in a solution that mimics a true clinical specimen (Fig. 6C). After

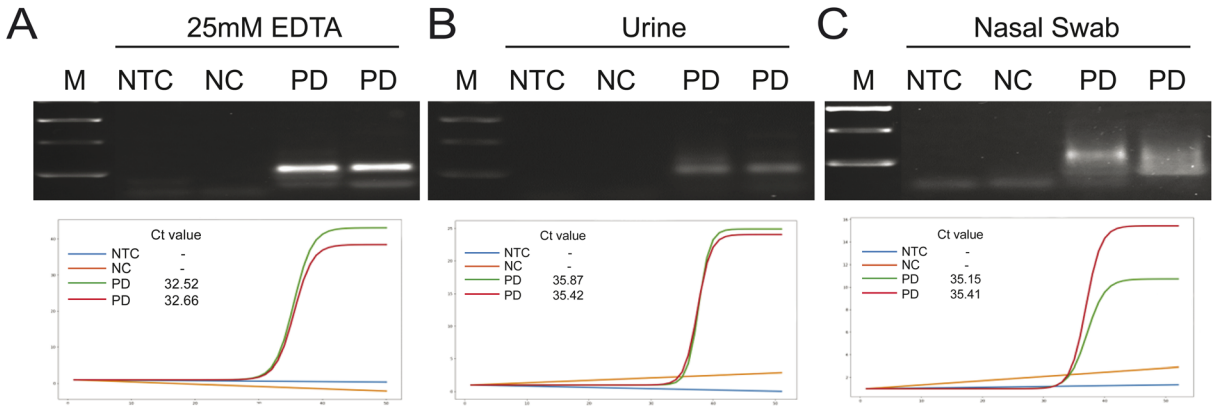

Fig. 6 AB1-5′Bio-15T pulldowns of S-protein expressing pseudovirus in complex solutions. Data illustrate agarose gel electrophoresis analysis and accompanying Kimera P-IV plasmonic RT-qPCRs (with C_t values) of AB pulldowns under PCR inhibitory conditions. (A) Pulldown in 25 mM of EDTA. (B) Pulldown in urine sample. (C) Pulldown on nasopharyngeal swab specimen. Abbreviations: NTC, no RNA template control; NC, no pulldown control; PD, pulldown.

thoroughly sampling both nostrils of a volunteer laboratory personnel, the flocked swab used was mixed and incubated in IP buffer before being spiked with 500 pseudovirus particles. Similarly, the AB pulldown was successful and yielded a C_t value of 35, whereas the no-pulldown control did not produce any detectable signal. The urine and nasopharyngeal swab pulldown experiments were performed using three different specimens and were reproducible; however, only duplicate experiments from a single individual are shown.

3.5 SARS-CoV-2 virus isolation

SARS-CoV-2 viruses were captured with the AB protocol, heat inactivated, lysed, and amplified in the Kimera P-IV platform by RT-PCR. Fig. 7 demonstrates the capture efficiency and amplification of these viruses compared to an unfunctionalized SMP control (bead control). AB1-5Bio+15T or non-functionalized SMPs were incubated in 1 mL of IP buffer with either 10^2 PFU or 10^5 PFU of SARS-CoV-2 virus for 30 minutes, followed by two washes with wash buffer, then two washes of IP buffer prior to RT-PCR analysis. The unexpected signal generated in the bead control (BC) lane is likely due to non-specific binding of the virus to the bare bead; however, the ABs demonstrate a significantly stronger signal than the bead control, indicating that the aptamers play a much larger role in capturing and effectively concentrating the viral particles from the sample than aptamer-bare SMPs. When amplifying the captured virions from the 10^5 PFU sample in the Kimera P-IV platform, fewer cycles were required to amplify a viral load of that titre. The ABs pulldown yielded C_t values of 17.94 and 18.09, and the bead control had no signal since there were not sufficient PCR cycles to properly amplify any residual virions non-specifically stuck to the SMPs' surfaces. Moreover, the RT-PCR was performed using only 25 cycles, and the detection was achieved in as little as 32 minutes. The pulldown protocol also demonstrated that it could isolate as low as 100 PFU, indicating substantial sensitivity below the limit of detection of other assays.[56] Our AB-targeted capture methodology has detection sensitivity similar to other protocols applying RNA

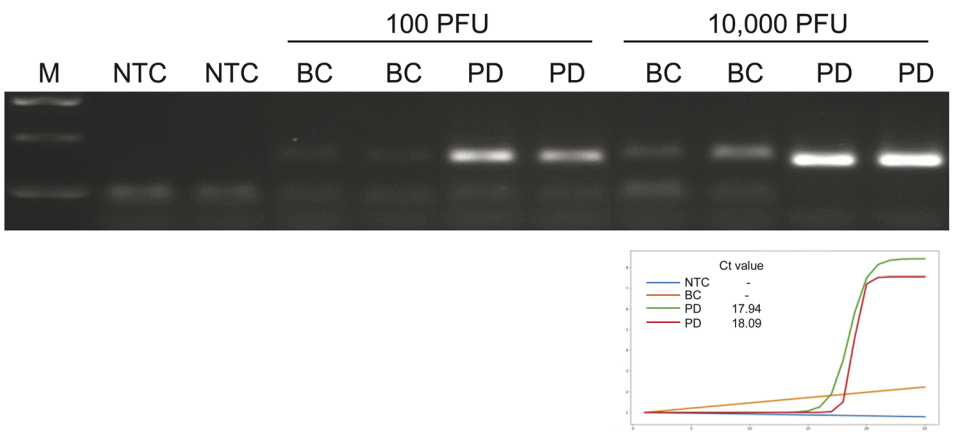

Fig. 7 AB pulldown of SARS-CoV-2 virus. Agarose gel electrophoresis analysis, accompanying Kimera P-IV plasmonic RT-qPCR output fluorescence curves with C_t values. These results highlight the capacity of the pulldown to detect real virus. Abbreviations: NTC, no RNA template control, BC, bead control referring to pulldown with unfunctionalized SMPs; PD, pulldown with AB.

extraction, which have described limits of detection ranging from 200 copies per mL to 10^6 copies per mL.[57–60]

It should be noted that the four wash steps removed most of the non-specific binding of virus to the SMPs themselves, although there was still some residual binding. While this may promote non-specific binding, this is not necessarily a disadvantage since these washes have already been shown to remove other PCR inhibitors. It should be noted that there are also other ways of decreasing the duration of the pulldown protocol, including reducing the incubation time of the ABs with the sample, diminishing the number of washes before performing RT-PCR, and optimizing the plasmonic PCR thermocycling parameters. Nonetheless, the complete pulldown process including plasmonic PCR analysis is still much faster than current automated nucleic acid isolation, coupled with improved sensitivity while purifying and concentrating the virus.

4. Conclusion

Our protocol demonstrated the ability to isolate 50 ng of recombinant Wuhan and Omicron variant SARS-CoV-2 spike protein in both ideal and complex solutions, and as little as 80 pseudoviral particle/1.5 mL s and 100 SARS-CoV-2 viruses. The ABs offer versatile applicability through adaptable functionalization with biotinylated aptamers to the surface of SMPs; however, our protocol can be vulnerable to rapidly evolving mutations of the virus which could impact on binding affinity to the S-protein, thus requiring updates to aptamer sequence to maintain detection sensitivity. Ultimately, we were able to demonstrate how viral isolation using ABs is an effective and sensitive method for sample preparation and concentration before RT-PCR analysis, offering a desirable workflow for a rapid POC diagnostics environment. Kondo *et al.*[61] investigated the use of antibody-like "monobodies", similarly attached to iron-beads, for targeted-capture of SARS-CoV-2 and showed a sensitivity of 1000–100 particles per mL. Other investigators have assessed a variety of particles to increase their sensitivity of targeted nucleic acid capture. Cui *et al.*[62] used poly-(amino ester) with carboxyl group-coated magnetic particles to target pseudoviral RNA and obtained a limit of detection of 100 copies per mL. Pang *et al.*[63] used Fe_3O_4@Ag magnetic particles for microRNA (miRNA) capture and attained a detection limit of roughly 90 miRNA copies per 50 μL reaction volume. Chen *et al.*[64] utilized magnetic particles to extract target material from solution and observed the changes in peroxidase activity of DNA/platinum – nanoparticle complexes through colorimetric assessment, achieving a limit of detection of 0.228 nM of material. Lastly, Tavallaie *et al.*[65] were able to confirm miRNA detection sensitivity of 10 aM by using complementary DNA probes on the surface of a gold microelectrode. Combining our ABs with the plasmonic qPCR platform improves on these methodologies incorporating magnetic particles in the sample capture and extraction process and to provide for an efficient, while also overcoming the inhibitory conditions of the sample media, and time-sensitive solution to bottlenecks in rapid point-of-care testing.

Author contributions

Conceptualization – MP, SV, and MAT; formal analysis – JH, AR, SSL, MY; experiments – JH, AR, MY; writing, review and editing – AR, JH, MP and MAT. All authors have read and agreed to the published version of the manuscript.

Conflicts of interest

MP and MAT are inventors of the following patent application: US9816132B2, Heating mechanism for DNA amplification, extraction or sterilization using photo-thermal nanoparticles; SSL, MP, and MAT are inventors of the following patent application: WO2020118444A, Ultraviolet quantitative label-free detection of DNA amplification.

Data availability

All data generated and analyzed during this study are available from the corresponding authors on reasonable request.

Supplementary information (SI): Data 1: (A) amplification and (B) melting curves of conventional PCR containing 25 μg SMPs ($n = 4$). Data 2: UV-Vis absorbance of different concentrations of SMP. See DOI: https://doi.org/10.1039/d6ay00498a.

Acknowledgements

Plasmonic Kimera P-IV point-of-care plasmonic qPCR machines used in our experiments were generously provided to us by Nexless Healthcare LP (Montreal, QC, Canada). The work was supported by a grant from the Canadian Institutes for Health Research (OV1-170654) and a generous donation from the Jewish General Hospital on behalf of Sophie Desmarais.

References

1 Worldometer - Coronvirus. Available from:https://www.worldometers.info/coronavirus/.
2 B. B. Abate, B. D. Tilahun and B. M. Yayeh, Global COVID-19 vaccine acceptance level and its determinants: an umbrella review, *BMC Public Health*, 2024, **24**(1), 5.
3 E. Karlafti, *et al.*, The Diagnostic Accuracy of SARS-CoV-2 Nasal Rapid Antigen Self-Test: A Systematic Review and Meta-Analysis, *Life*, 2023, **13**(2), 281.
4 G. O. Canada Testing for COVID-19: When to get tested and testing results. Available from: https://www.canada.ca/en/public-health/services/diseases/2019-novel-coronavirus-infection/symptoms/testing/diagnosing.html.
5 T. Olanipekun, The impact of COVID-19 testing on length of hospital stay and patient flow in hospitals, *J. Community Hosp. Intern. Med. Perspect.*, 2021, **11**(2), 180–183.
6 R. Filip, *et al.*, Global Challenges to Public Health Care Systems during the COVID-19 Pandemic: A Review of Pandemic Measures and Problems, *J. Pers. Med.*, 2022, **12**(8), 1295.
7 D. Sharma, *et al.*, In silico evaluation of the impact of Omicron variant of concern sublineage BA.4 and BA.5 on

the sensitivity of RT-qPCR assays for SARS-CoV-2 detection using whole genome sequencing, *J. Med. Virol.*, 2023, **95**(1), e28241.

8 G. Hansen, *et al.*, Clinical Performance of the Point-of-Care cobas Liat for Detection of SARS-CoV-2 in 20 Minutes: a Multicenter Study, *J. Clin. Microbiol.*, 2021, **59**(2), e02811.

9 S. More, *et al.*, Pooling of Nasopharyngeal Swab Samples To Overcome a Global Shortage of Real-Time Reverse Transcription-PCR COVID-19 Test Kits, *J. Clin. Microbiol.*, 2021, **59**(4), e01295.

10 B. Arezi, M. McCarthy and H. Hogrefe, Mutant of Moloney murine leukemia virus reverse transcriptase exhibits higher resistance to common RT-qPCR inhibitors, *Anal. Biochem.*, 2010, **400**(2), 301–303.

11 B. C. Hudson, *et al.*, The effects of dithiothreitol (DTT) on fluorescent qPCR dyes, *J. Forensic Sci.*, 2021, **66**(2), 700–708.

12 X. J. Lou, *et al.*, Increased amplification efficiency of microchip-based PCR by dynamic surface passivation, *Biotechniques*, 2004, **36**(2), 248–252.

13 N. M. Adams, *et al.*, Comparison of three magnetic bead surface functionalities for RNA extraction and detection, *ACS Appl. Mater. Interfaces*, 2015, **7**(11), 6062–6069.

14 D. Avetyan, *et al.*, SARS-CoV-2 detection by extraction-free qRT-PCR for massive and rapid COVID-19 diagnosis during a pandemic in Armenia, *J. Virol. Methods*, 2021, **295**, 114199.

15 C. M. Victoriano, *et al.*, Direct PCR with the CDC 2019 SARS-CoV-2 assay: optimization for limited-resource settings, *Sci. Rep.*, 2022, **12**(1), 11756.

16 V. Marie and M. L. Gordon, The (Re-)Emergence and Spread of Viral Zoonotic Disease: A Perfect Storm of Human Ingenuity and Stupidity, *Viruses*, 2023, **15**(8), 1683.

17 J. Hayes, *et al.*, Performance and functional assessment of the Kimera P-IV point-of-care plasmonic qPCR prototype for ultra rapid pathogen detection of chlamydia trachomatis, *Epidemiol. Infect.*, 2025, **153**, e27.

18 I. Brukner, *et al.*, Assessing Different PCR Master Mixes for Ultrarapid DNA Amplification: Important Analytical Parameters, *Diagnostics*, 2024, **14**(5), 477.

19 A. S. Peinetti, *et al.*, Direct detection of human adenovirus or SARS-CoV-2 with ability to inform infectivity using DNA aptamer-nanopore sensors, *Sci. Adv.*, 2021, **7**(39), eabh2848.

20 L. Shi, *et al.*, Aptamer-Functionalized Nanochannels for One-Step Detection of SARS-CoV-2 in Samples from COVID-19 Patients, *Anal. Chem.*, 2021, **93**(49), 16646–16654.

21 Y. Song, *et al.*, Discovery of Aptamers Targeting the Receptor-Binding Domain of the SARS-CoV-2 Spike Glycoprotein, *Anal. Chem.*, 2020, **92**(14), 9895–9900.

22 G. Yang, *et al.*, Identification of SARS-CoV-2-against aptamer with high neutralization activity by blocking the RBD domain of spike protein 1, *Signal Transduct. Targeted Ther.*, 2021, **6**(1), 227.

23 S. Balamurugan, *et al.*, Effect of Linker Structure on Surface Density of Aptamer Monolayers and Their Corresponding Protein Binding Efficiency, *Anal. Chem.*, 2008, **80**(24), 9630–9634.

24 S. Ni, *et al.*, Chemical Modifications of Nucleic Acid Aptamers for Therapeutic Purposes, *Int. J. Mol. Sci.*, 2017, **18**(8), 1683.

25 B. Waybrant, T. R. Pearce and E. Kokkoli, Effect of Polyethylene Glycol, Alkyl, and Oligonucleotide Spacers on the Binding, Secondary Structure, and Self-Assembly of Fractalkine Binding FKN-S2 Aptamer-Amphiphiles, *Langmuir*, 2014, **30**(25), 7465–7474.

26 D. Patel, New human angiotensin converting enzyme 2 (ACE2) knock-in CD-1 mouse model of asymptomatic SARS-CoV-2 infection, in *Department of Human Genetics*, McGill University, 2022.

27 C. Chakraborty, *et al.*, The D614G mutation helps to increase the transmissibility and reduce the virulence of SARS-CoV-2 variants through natural selection, *Int. J. Surg.*, 2023, **109**(2), 171–174.

28 J. Li, *et al.*, Diverse high-affinity DNA aptamers for wild-type and B.1.1.7 SARS-CoV-2 spike proteins from a pre-structured DNA library, *Nucleic Acids Res.*, 2021, **49**(13), 7267–7279.

29 S. Klein, *et al.*, SARS-CoV-2 structure and replication characterized by in situ cryo-electron tomography, *Nat. Commun.*, 2020, **11**(1), 5885.

30 M. Laue, *et al.*, Morphometry of SARS-CoV and SARS-CoV-2 particles in ultrathin plastic sections of infected Vero cell cultures, *Sci. Rep.*, 2021, **11**(1), 3515.

31 O. Puhach, B. Meyer and I. Eckerle, SARS-CoV-2 viral load and shedding kinetics, *Nat. Rev. Microbiol.*, 2023, **21**(3), 147–161.

32 J. P. Brody, *et al.*, Biotechnology at low Reynolds numbers, *Biophys. J.*, 1996, **71**(6), 3430–3441.

33 C. T. Wittwer, G. C. Fillmore and D. J. Garling, Minimizing the time required for DNA amplification by efficient heat transfer to small samples, *Anal. Biochem.*, 1990, **186**(2), 328–331.

34 J. N. Anker, *et al.*, Biosensing with plasmonic nanosensors, *Nat. Mater.*, 2008, **7**(6), 442–453.

35 L. Tang, J. Casas and M. Venkataramasubramani, Magnetic Nanoparticle Mediated Enhancement of Localized Surface Plasmon Resonance for Ultrasensitive Bioanalytical Assay in Human Blood Plasma, *Anal. Chem.*, 2013, **85**(3), 1431–1439.

36 K. A. Willets and R. P. Van Duyne, Localized surface plasmon resonance spectroscopy and sensing, *Annu. Rev. Phys. Chem.*, 2007, **58**, 267–297.

37 E. Carrasco, *et al.*, Plasmonic Hot-Electron Reactive Oxygen Species Generation: Fundamentals for Redox Biology, *Front. Chem.*, 2020, **8**, 591325.

38 L. Gao, *et al.*, Plasmon-mediated generation of reactive oxygen species from near-infrared light excited gold nanocages for photodynamic therapy in vitro, *ACS Nano*, 2014, **8**(7), 7260–7271.

39 M. S. Cooke, *et al.*, Oxidative DNA damage: mechanisms, mutation, and disease, *FASEB J.*, 2003, **17**(10), 1195–1214.

40 L. J. Marnett, Oxyradicals and DNA damage, *Carcinogenesis*, 2000, **21**(3), 361–370.

41 S. S. Wallace, Biological consequences of free radical-damaged DNA bases, *Free Radic. Biol. Med.*, 2002, **33**(1), 1–14.

42 D. Wang, D. A. Kreutzer and J. M. Essigmann, Mutagenicity and repair of oxidative DNA damage: insights from studies using defined lesions, *Mutat. Res.*, 1998, **400**(1–2), 99–115.
43 J. A. Sikorsky, *et al.*, Effect of DNA damage on PCR amplification efficiency with the relative threshold cycle method, *Biochem. Biophys. Res. Commun.*, 2004, **323**(3), 823–830.
44 S. H. Hwang, *et al.*, Effects of upconversion nanoparticles on polymerase chain reaction, *PLoS One*, 2013, **8**(9), e73408.
45 W. Wan and J. T. Yeow, The effects of gold nanoparticles with different sizes on polymerase chain reaction efficiency, *Nanotechnology*, 2009, **20**(32), 325702.
46 Z. Yang, *et al.*, Application of Nanomaterials to Enhance Polymerase Chain Reaction, *Molecules*, 2022, **27**(24), 8854.
47 G. Rivas and A. P. Minton, Macromolecular Crowding In Vitro, In Vivo, and In Between, *Trends Biochem. Sci.*, 2016, **41**(11), 970–981.
48 M. Sidstedt, P. Rådström and J. Hedman, PCR inhibition in qPCR, dPCR and MPS—mechanisms and solutions, *Anal. Bioanal. Chem.*, 2020, **412**(9), 2009–2023.
49 Z. Zhang, *et al.*, High-Affinity Dimeric Aptamers Enable the Rapid Electrochemical Detection of Wild-Type and B.1.1.7 SARS-CoV-2 in Unprocessed Saliva, *Angew Chem. Int. Ed. Engl.*, 2021, **60**(45), 24266–24274.
50 R. Sender, *et al.*, The total number and mass of SARS-CoV-2 virions, *Proc. Natl. Acad. Sci. U. S. A.*, 2021, **118**(25), e2024815118.
51 Y. Bai, *et al.*, Enhancing the Affinity of Anti-Human alpha-Thrombin 15-mer DNA Aptamer and Anti-Immunoglobulin E Aptamer by PolyT Extension, *Anal. Chem.*, 2017, **89**(17), 9467–9473.
52 Q. Yang, *et al.*, Just 2% of SARS-CoV-2-positive individuals carry 90% of the virus circulating in communities, *Proc. Natl. Acad. Sci. U. S. A.*, 2021, **118**(21), e2104547118.
53 B. R. Lawaju and G. Yan, Assessment of Common Factors Associated with Droplet Digital PCR (ddPCR) Quantification of Paratrichodorus allius in Soil, *Int. J. Mol. Sci.*, 2024, **25**(6), 3104.
54 A. Mori, *et al.*, Urine: A Pitfall for Molecular Detection of Toscana Virus? An Analytical Proof-of-Concept Study, *Viruses*, 2024, **16**(1), 98.
55 B. Ebner, *et al.*, The COVID-19 pandemic - what have urologists learned?, *Nat. Rev. Urol.*, 2022, **19**(6), 344–356.
56 R. Arnaout, *et al.*, The Limit of Detection Matters: The Case for Benchmarking Severe Acute Respiratory Syndrome Coronavirus 2 Testing, *Clin. Infect. Dis.*, 2021, **73**(9), e3042–e3046.
57 M. Laverack, *et al.*, Clinical evaluation of a multiplex real-time RT-PCR assay for detection of SARS-CoV-2 in individual and pooled upper respiratory tract samples, *Arch. Virol.*, 2021, **166**(9), 2551–2561.
58 H. Jayakody, *et al.*, Development of a high sensitivity RT-PCR assay for detection of SARS-CoV-2 in individual and pooled nasopharyngeal samples, *Sci. Rep.*, 2022, **12**(1), 5369.
59 Y. Jiang, *et al.*, Establishment of a quantitative RT-PCR detection of SARS-CoV-2 virus, *Eur. J. Med. Res.*, 2021, **26**(1), 147.
60 M. S. Muller, *et al.*, Practical strategies for SARS-CoV-2 RT-PCR testing in resource-constrained settings, *Diagn. Microbiol. Infect. Dis.*, 2021, **101**(2), 115469.
61 T. Kondo, *et al.*, Antibody-like proteins that capture and neutralize SARS-CoV-2, *Sci. Adv.*, 2020, **6**(42), eabd3916.
62 H. Cui, *et al.*, A simplified viral RNA extraction method based on magnetic nanoparticles for fast and high-throughput detection of SARS-CoV-2, *Talanta*, 2023, **258**, 124479.
63 Y. Pang, *et al.*, Fe(3)O(4)@Ag magnetic nanoparticles for microRNA capture and duplex-specific nuclease signal amplification based SERS detection in cancer cells, *Biosens. Bioelectron.*, 2016, **79**, 574–580.
64 W. Chen, *et al.*, DNA-mediated inhibition of peroxidase-like activities on platinum nanoparticles for simple and rapid colorimetric detection of nucleic acids, *Biosens. Bioelectron.*, 2017, **94**, 169–175.
65 R. Tavallaie, *et al.*, Nucleic acid hybridization on an electrically reconfigurable network of gold-coated magnetic nanoparticles enables microRNA detection in blood, *Nat. Nanotechnol.*, 2018, **13**(11), 1066–1071.